Emodin improves renal fibrosis in chronic kidney disease by regulating mitochondrial homeostasis through the mediation of peroxisome proliferator-activated receptor-gamma coactivator-1 alpha (PGC-1α)

Liuchang Feng,[1]* Zaoqiang Lin,[1]* Zeyong Tang,[2] Lin Zhu,[1,3] Shu Xu,[4] Xi Tan,[5] Xinyuan Wang,[6] Jianling Mai,[7] Qinxiang Tan[1]

[1]Department of Nephrology, Shenzhen Hospital, Beijing University of Chinese Medicine, Shenzhen
[2]Department of Nephrology, Guangzhou University of Chinese Medicine, Guangzhou
[3]Department of Nephrology, Dongzhimen Hospital, Beijing University of Chinese Medicine, Beijing
[4]Department of Oncology, Shenzhen Hospital, University of Chinese Academy of Sciences, Shenzhen
[5]Medicopsychology, Shenzhen Hospital, Beijing University of Chinese Medicine, Shenzhen
[6]Medicopsychology, School of Life Sciences, Beijing University of Chinese Medicine, Beijing
[7]Department of Hemodialysis, Guangdong Provincial Hospital of Chinese Medicine, Guangzhou, China

*These authors contributed equally to this work.

ABSTRACT

Chronic kidney disease (CKD) is a leading public health issue associated with high morbidity worldwide. However, there are only a few effective therapeutic strategies for CKD. Emodin, an anthraquinone compound from rhubarb, can inhibit fibrosis in tissues and cells. Our study aims to investigate the antifibrotic effect of emodin and the underlying molecular mechanism. A unilateral ureteral obstruction (UUO)-induced rat model was established to evaluate the effect of emodin on renal fibrosis development. Hematoxylin and eosin staining, Masson's trichrome staining, and immunohistochemistry staining were performed to analyze histopathological changes and fibrotic features after emodin treatment. Subsequently, a transforming growth factor-beta 1 (TGF-β1)-induced cell model was used to assess the inhibition of emodin on cell fibrosis *in vitro*. Furthermore, Western blot analysis and real-time quantitative reverse transcription-polymerase chain reaction were performed to validate the regulatory mechanism of emodin on renal fibrosis progression. As a result, emodin significantly improved histopathological abnormalities in rats with UUO. The expression of fibrosis biomarkers and mitochondrial biogenesis-related proteins also decreased after emodin treatment. Moreover, emodin blocked TGF-β1-induced fibrotic phenotype, lipid accumulation, and mitochondrial homeostasis in NRK-52E cells. Conversely, peroxisome proliferator-activated receptor-gamma coactivator-1 alpha (PGC-1α) silencing significantly reversed these features in emodin-treated cells. Collectively, emodin plays an important role in regulating PGC-1α-mediated mitochondria function and energy homeostasis. This indicates that emodin exhibits great inhibition against renal fibrosis and acts as a promising inhibitor of CKD.

Key words: emodin; PGC-1α; chronic kidney disease; mitochondrial homeostasis.

Correspondence: Qinxiang Tan, Department of Nephrology, Shenzhen Hospital, Beijing University of Chinese Medicine, No.1 Dayun Road, Longgang District, Shenzhen 518116, China. E-mail: qinxiangtan2023@163.com

Contributions: ZL, LF, QT, study concept and design; ZT, LZ, SX, contribution to kidney and blood collection, partial animal experiments; XT, XW, JM, data collection and statistical analysis; ZL, LF, manuscript original drafting; QT, manuscript revision and editing. All the authors read and approved the final version of the manuscript and agreed to be accountable for all aspects of the work..

Conflict of interest: the authors declare that they have no competing interests, and all authors confirm accuracy.

Ethical approval: all animal experiments were conducted with protocols approved by the Experimental Animal Ethics Committee of Shenzhen Hospital of Beijing University of Traditional Chinese Medicine (no. SZLDH2020LSYA-086).

Availability of data and materials: the data supporting the findings of this study are available from the corresponding author upon reasonable request.

Funding: this study was supported by the Yulong Talent Training Program at Shenzhen Hospital of Beijing University of Traditional Chinese Medicine (2020-BUCMSZYLRC02).

Introduction

Chronic kidney disease (CKD) is a major public health issue with a 13.4% of worldwide incidence rate, which affects more than 800 million individuals.[1,2] If preventive strategies are not undertaken, CKD can develop into end-stage renal disease and cardiovascular disease, leading to ahigh mortality and global CKD-related burden.[3,4] Renal tubulointerstitial fibrosis is a common outcome of advanced-stage CKD, which ultimately contributes to renal failure.[5] Renal interstitial fibrosis is characterized by renal tubular atrophy, inflammatory cell infiltration, fibroblast accumulation, and interstitial matrix deposition.[6,7] Animal models of renal fibrosis contains surgical- or drug-induced model, spontaneous model, transgenic modification model, and complex model.[8] The unilateral ureteral obstruction (UUO)-induced animal model is a mature surgical-induced model that is widely used in understanding the pathophysiological mechanisms of obstructive kidney disease.[9] Generally, UUO-induced animals have features such as renal tubular dilation, interstitial hyperplasia, proximal renal tubular injury, and hydronephrosis, leading to renal scar formation and interstitial fibrosis.[10] Compared with other *in vivo* models, UUO has more advantages, including easy to perform, a short cycle, and a high survival rate. Further, UUO-induced renal fibrosis is lower exogenous toxins and uremic environment. Therefore, it is a reasonable model for preclinical studies.[8] Numerous studies based on a UUO-induced model have revealed many molecular pathways involved in renal fibrosis.[11-13] Cellular events, such as inflammation, fibroblast activation, epithelial-to-mesenchymal transition, tubular injury, peritubular capillary rarefaction, and hypoxia, are all associated with renal fibrogenesis.[11] Among the molecular bases involved in renal fibrosis, transforming growth factor-beta 1 (TGF-β1)/Smad signaling is one of the important nodes.[13,14]

Mitochondrial impairment is a primary risk factor in kidney disorders with fibrosis development.[15] PGC-1α can drive some transcriptional molecules to regulate mitochondrial biogenesis and downstream metabolic pathways.[16] PGC-1α inactivated NOD-like receptor family-pyrin domain containing three inflammasomes, which improved kidney damage in UUO-treated mice.[17] Moreover, PGC-1α plays a unique role in regulating mitochondrial transcription factor A (Tfam) in kidney fibrosis.[18] Furthermore, PGC-1α inhibited metabolic dysregulation in Notch-associated kidney fibrosis.[19] Therefore, PGC-1α might be a promising target for therapeutic strategies against CKD development.

Emodin is a bioactive component extracted from rhubarb and a significant clinical efficacy.[20] It has good antifibrotic effects in both UUO- and surgery-induced renal fibrosis. The mechanisms underlying these studies were associated with TGF-β1/Smad signaling.[21,22] In addition, it inhibits renal tubulointerstitial fibrosis *via* interacting with EZH2, a histone methyltransferase.[23] However, effects of emodin on regulating PGC-1α have not been reported yet.

The purpose of this study was to investigate the effect of emodin on both UUO-induced renal fibrosis *in vivo* and TGF-β1-induced cell fibrosis *in vitro*.

Materials and Methods

Cell culture and treatment

Rat renal tubular duct epithelial (NRK-52E) cells were purchased from Jennio Biotech (Guangzhou, China). Cells were cultured in Dulbecco's Modified Eagle Medium (Invitrogen, Carlsbad, CA, USA) supplemented with 10% fetal bovine serum (FBS, Gibco, Carlsbad, CA, USA), 100 μg/mL of streptomycin, and 100 U/mL of penicillin. The cells were kept in an incubator at 37°C with 5% carbon dioxide. TGF-β1 can trigger cell fibrosis in progressive kidney disease, and TGF-β1-mediated signaling act a central role in renal fibrosis.[24] Here, we used TGF-β1 to drive fibrosis in NRK-52E cells. Specifically, When the cells had grown to 80%confluence, they were starved overnight in Roswell Park Memorial Institute 1640 (RPMI 1640) supplemented with 0.5% FBS before being exposed to 10 ng/mL TGF-β1 in the presence or absence of 25, 50, or 100 μM emodin for 24 h.

Short interfering RNA and transfection

Short interfering RNA (siRNA) oligonucleotides against peroxisome proliferator-activated receptor-gamma coactivator-1 alpha (PGC-1α) and negative controls were synthesized by Sangon Biotech Co., Ltd. (Shanghai, China), and then transiently transfected into NRK-52E cells using Lipofectamine 2000 (Invitrogen). The siRNA oligonucleotide sequences were as follows: PGC-1α siRNA, sense: 5′-GATGTGAACGACTTGGATACA-3′, control siRNA, sense: 5′-UUCUCCGAACGUGUCACGU-3′.

Animals and UUO-induced rat model

Male Sprague-Dawley rats (250±20 g) were purchased from the Animal Center of Southern Medical University (Guangzhou, China) and raised in a specified pathogen-free facility. Rats were maintained in a standard condition (humidity: 50%, temperature: 22°C) with a 12-h light-dark cycle and had free access to food and water. All animal protocols were approved by the Institutional Animal Care and Use Committee of Shenzhen Hospital of Beijing University of Traditional Chinese Medicine (no. SZLDH2020LSYA-086). To establish the UUO rat model, rats were anesthetized with 1% pentobarbital sodium (40 mg/kg) at first. Then, the unilateral abdominal incision was performed to expose and ligate the left ureter with 6-0 silk at two points. Finally, the ureter between the two ligation points was cut. The sham-operated group did not undergo ligation. Rats were randomly divided into four groups (n=6): i) sham-operated rats (sham), ii) UUO rats with vehicle (0.5% CMC-Na alone as the vehicle), iii) UUO rats treated with emodin (emodin 30 mg/kg in 0.5% CMC-Na), and iv) UUO rats treated with fenofibrate (Feno 100 mg/kg in 0.5% CMC-Na). Fenofibrate has great renoprotective effect on tubulointerstitial inflammation and fibrosis,[25] which was served as a positive control in this study. One week after UUO surgery, the rats were administered with emodin and fenofibrate daily for 6 weeks. At the end of the experiment, rats were euthanized with 3% pentobarbital sodium (150 mg/kg). The kidneys were excised and then stored inside a freezer with a temperature of -80°C or fixed in 4% paraformaldehyde for further experiments.

Hematoxylin & eosin staining

Paraffin kidney tissue sections were dewaxed and hydrated, and then stained with hematoxylin and eosin (H&E) solution (Sigma Aldrich). After the slices were dried, they were preserved with neutral resin.

Ten non-repeating fields were randomly selected. Tubulointerstitial lesions were scored from 0 to 5 according to the following positive signal intensities: 0, normal; 1, mild (<25% of the cortex); 2, moderate (25-50%); 3, severe (50-75%); and 4, extensive damage (>75%). The pathology score was used to assess the degree of tubulointerstitial fibrosis.

Masson's trichrome staining

Kidney tissue sections were stained using the Masson's Trichrome Stain Kit (Servicebio Technology Co., Ltd., Wuhan, China). The slides were deparaffinized and hydrated and then incu-

bated in Masson A overnight. Then, they were washed with running tap water. The tissue sections were stained with mixed liquor of Masson B and Masson C for 1 min and differentiated by incubating the slides with 1% hydrochloric acid. The slides were successively incubated in Masson D, Masson E, and Masson F before differentiation and dehydration. Finally, the slides were cleared in xylene and mounted with neutral resin. Histological features were observed using a light microscope equipped with a digital camera (Nikon, Kanagawa, Japan), where collagenous fiber was stained in blue. The areas with blue staining were analyzed by ImageJ (NIH).

Immunochemistry

Paraffin kidney tissue slices were dewaxed, rehydrated, and then incubated with primary antibodies, including anti-PGC-1α (1:100, Abcam, Cambridge, MA, USA), anti-smooth muscle alpha-actin (α-SMA) (1:100, Abcam), anti-mitochondrial transcription factor A (Tfam) (1:100, Cell Signaling Technology, Danvers, MA, USA), fibronectin (1:100, Abcam), anti-collagen type I alpha 1 chain (COL1A1) (1:100, Abcam), anti-long-chain acyl-CoA dehydrogenase (LCAD) (1:100, Abcam), and anti-MCAD (1:100, Abcam), overnight at 4°C, followed by secondary antibody (1:200; Cell Signaling Technology). Subsequently, the sections were successively stained with 3,3'-Diaminobenzidine (DAB) and hematoxylin. Non-specific immunoglobulin and no primary antibody were served as negative controls. Images were taken using a light microscope (XSP-C204, CIC). The signaling intensity was measured with ImageJ (NIH). For each sample, the average value was calculated through calculating 5 non-overlapping fields (4x magnification) as a percentage of the analyzed total area.

Cell counting kit-8 assay

Cells were seeded into 96-well plates. After treatment, 10 μL of the cell counting kit-8 (CCK8) reagent (Sigma Aldrich) per well was added and incubated at 37°C for 4 h. Absorbance at 450 nm was examined using a microplate reader (Bio-Rad Laboratories, Benicia, CA, USA).

Oil Red O staining

The cell culture medium was discarded, and then cells were fixed in 4% paraformaldehyde for half an hour. After washing twice with phosphate-buffered saline. A 60% of Oil Red O (Beyotime Biotech, Shanghai, China) solution was used to incubate the fixed cells for 10-20 min. Next, the cells were rinsed twice with phosphate-buffered saline. The stained lipid droplets in the cytoplasm were observed using an optical microscope (XSP-C204, CIC, 40x magnification). For each sample, the cells stained with Oil Red O were counted, and the average value was calculated by 5 non-overlapping fields as a percentage of total cells in the analyzed area.

Quantitative real-time PCR

Total RNA was extracted from tissues or cells using TRIzol reagent (Beyotime Biotech), according to the manufacturer's instructions. Reverse transcription was performed using M-MLV Reverse Transcriptase (Promega, Madison, WI, USA). Complementary DNA was examined using quantitative real-time reverse transcription-polymerase chain reaction on the Power SYBR Green PCR Master Mix (Applied Biosystems, Foster City, CA, USA). Relative gene expressions were calculated using the 2-ΔΔCt method. β-actin was used as an internal reference. The primers were as follow: Pparpgc1α primers: forward 5' AACATTCAAAGCAGCAGAGAGG 3', reverse 5'-AAGTTCTTCGTACAGCCATCAA-3'; αSma primers: forward 5'-TTCCTTTGCCTATCAGAATGG-3', reverse 5'-TCCTTAACCACAGATCCAATTC-3'; fibronectin primers: forward 5'-TTACACGGTTTCCCATTACGC-3', reverse 5'-TCGCATCTGAAATGACCACTG-3'; Tfam primers: forward 5'-AGACAGGGTTTCTCTGCGTTG-3', reverse 5'-CAGTGACAGGCTGGTGGCAA-3'; Col1a1 primers: forward 5'-CTCGTTCTTGTCTTTGTGTGTCA-3', reverse 5'-CCTTCACAGAGATGTAGCACCTT-3'; Lcad primers: forward 5'-GCTAGACATCTGCCTACATCCTG-3', reverse 5'-TTTCTCTCTCCCTGTGTTAATCT-3'; Mcad primers: forward 5'-CTGATGAGGGACGCCAAGA-3', reverse 5'-CTTAGTTACACGAGGGTGATGC-3'.

Western blot analysis

Tissues and cells were lysed using RIPA lysis buffer (Beyotime Biotech) to obtain total protein. The protein concentration was quantified using the BCA Kit (Beyotime Biotech). The aliquot of proteins was subjected to sodium dodecyl sulfate-polyacrylamide gel electrophoresis and was transferred onto the polyvinylidene fluoride membrane. The membrane was blocked with 5% skim milk for 2 h and then incubated with primary antibodies, including PGC-1α (1:1000, Abcam), α-SMA (1:1000, Abcam), Tfam (1:1000, Cell Signaling Technology), fibronectin (1:1000, Abcam), COL1A1 (1:1000, Abcam), LCAD (1:1000, Abcam), and MCAD (1:1000, Abcam), overnight at 4°C. Glyceraldehyde-3-phosphate dehydrogenase (1:10000; Abcam) was used as an internal control. Subsequently, the membrane was hybridized with horseradish peroxidase-conjugated secondary antibody (1:5000, Cell Signaling Technology). The immunoreactive bands were measured using the enhanced chemiluminescent kit.

Quantification of mitochondrial DNA content

Total cellular DNA was extracted using the DNA Isolation Mini Kit (Vazyme, Nanjing, Jiangsu, China), according to the manufacturer's instructions. The mtDNA copy number on qPCR was detected with TaqMan Universal PCR Master Mix and various primers (16S rRNA primers: forward 5'-CATTGCTGACAGGATGCAGAAGG-3', reverse 5'-TGCTGGAAGGTGGACAGTGAGG-3'; 18S rRNA primers: forward 5'-CAGCCACCCGAGATTGAGCA-3', reverse 5'-TAGTAGCGACGGGCGGTGTG-3'). The MtDNA levels were evaluated using the mitochondrial genes 16S rRNA, and the nuclear 18S rRNA was used as a loading control.

Mitochondrial membrane potential

The JC-1 kit (Beyotime Biotechnology) was used to determine mitochondrial membrane potential, according to the manufacturer's guidelines. After treatment with 10 ng/mL TGF-β1 or 10 ng/mL TGF-β1+ 100 μM emodin, The cells were resuscitated in 500 μL of JC-1 staining solution and then incubated in a 5% CO2 incubator at 37°C for 20 min. After centrifugation for 4 min, cells were collected and washed twice with JC-1 staining buffer. The cells were then resuspended in an appropriate amount of JC-1 staining buffer. The results were expressed as JC - 1 red / green fluorescence. In normal cells, JC-1 dye enters the mitochondrial matrix, forms JC-1 aggregates, and fluoresces red. When the mitochondrial membrane potential is low, JC-1 dye exists mainly in the monomeric form, emitting green fluorescence. The cells were directly imaged using a fluorescent inverted microscope with a digital camera (BX53M, Olympus, Tokyo, Japan).

Total adenosine triphosphate

The total adenosine triphosphate (ATP) was quantified using the commercially available ATP Assay Kit (BioVision, Milpitas, CA, USA). After treatment, cells were collected and subsequently lysed with lysis buffer according to the instruction of the ATP

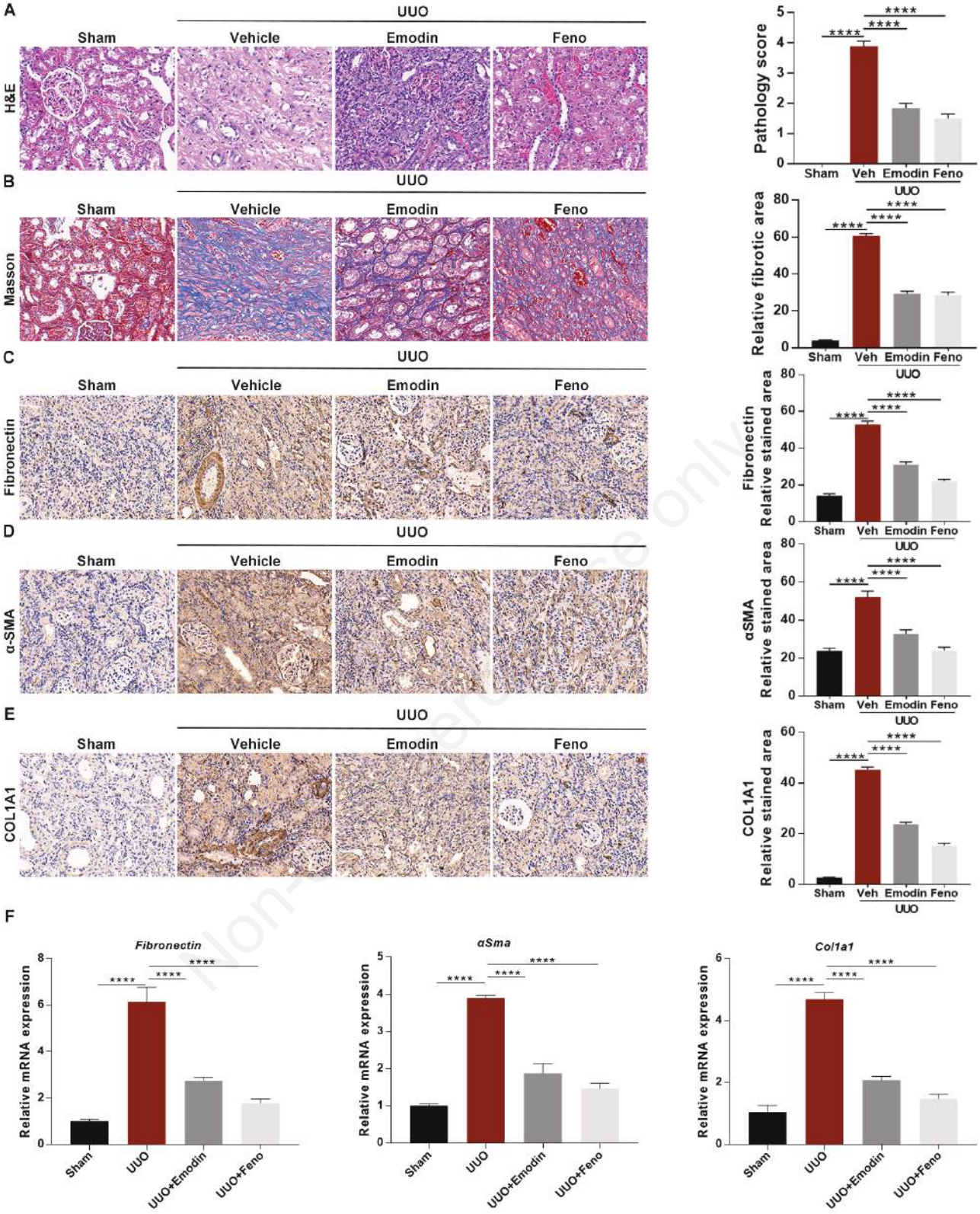

Figure 1. Emodin improves UUO-induced renal injury and fibrosis. **A-D**) Histological changes were evaluated *via* H&E staining and Masson's trichrome staining. **C-E**) Levels of fibronectin, smooth muscle alpha-actin (α-SMA), and collagen type I alpha 1 chain (COL1A1) were measured via immunohistochemical staining to assess fibrosis. The pathological scores were also calculated. **F**) th mRNA level of *fibronectin, α–Sma,* and *Col1a1* was detected. Data were expressed as mean ±SD (n=6);. **p*<0.05, ***p*<0.01, ****p*<0.001, *****p*<0.001.

Assay Kit. Then, 10 μL of lysates were added into 100 μL of ATP reaction solution that consists of D-Luciferin, luciferase, and buffer. Then, the mixture was incubated for 15-20 min at room temperature. For each group, there were 5 repeats. The luminescence was assessed using the EnVision microplate reader (Perkin Elmer, Waltham, MA, USA).

Transmission electron microscopy

Cells were collected and fixed in 1.25% glutaraldehyde (0.1 mol/L). Ultrathin sections (60 nm) were prepared using a microtome, placed on copper grids, and stained with uranyl acetate and lead citrate. Then, the sections were observed under an electron microscope (JEOL JEM-1010, Tokyo, Japan).

Detection of intra-mitochondrial ROS

Cells were treated with 10 ng/mL TGF-β1, or 10 ng/mL TGF-β1+ 100 μM emodin. Negative control was no-treatment group. After 24 h, cells were collected using 0.25% trypsin and maintained in a tube with completed medium. Subsequently, the ROS level in cells were analyzed using a ROS Testing Kit (Beoytime Biotech). Those cells with ROS signal were counted by a FACSCalibur flow cytometer (BD Biosciences, San Jose, CA, USA).

Statistical analysis

Statistical analysis was performed using GraphPad Prism 7. The differences between multiple groups were evaluated using

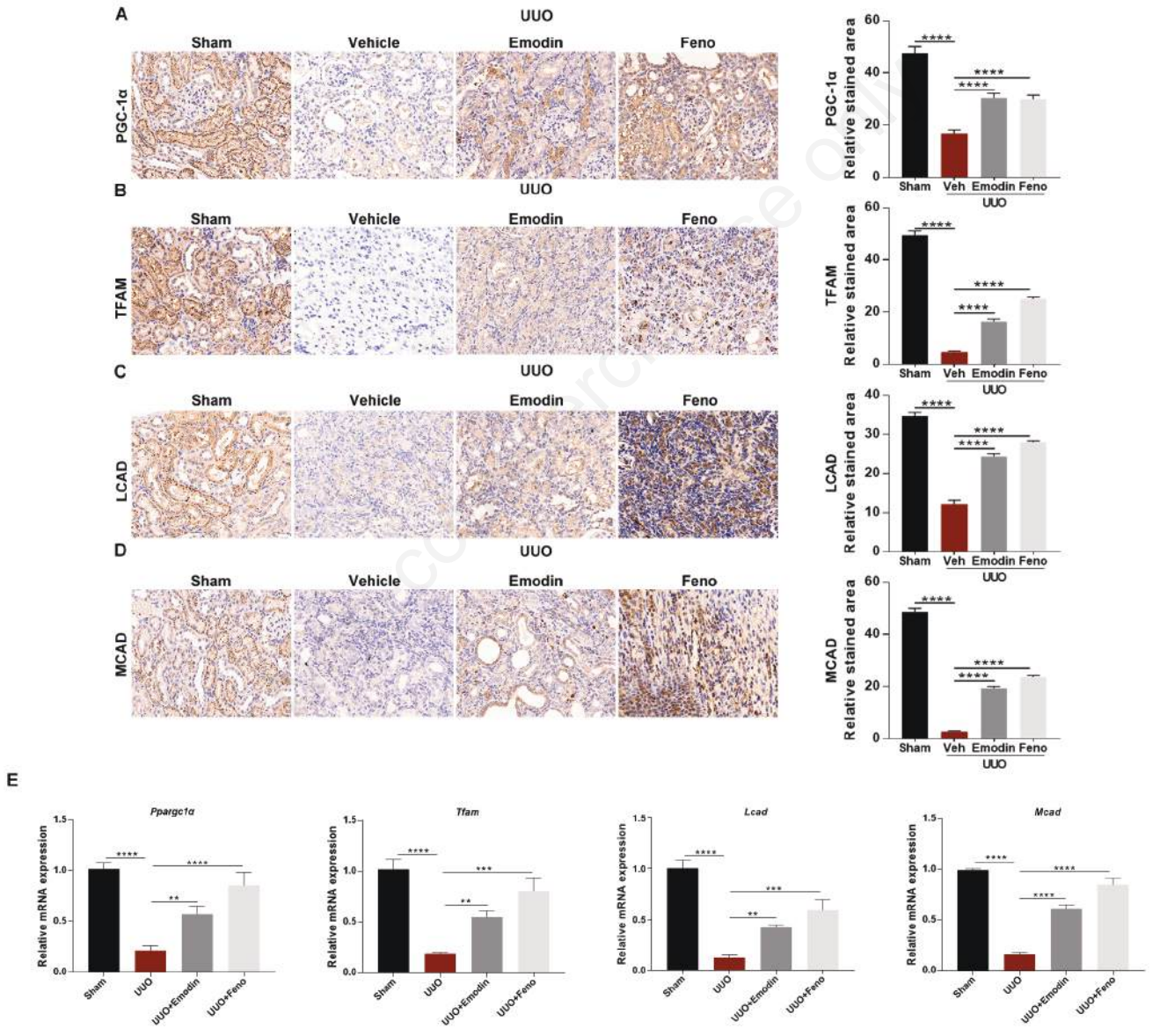

Figure 2. Emodin facilitated mitochondrial homeostasis in UUO-induced rats. **A-E**) The representative immunohistochemical images and pathological scores of peroxisome proliferator-activated receptor-gamma coactivator-1 alpha (PGC-1α), mitochondrial transcription factor A (Tfam), long-chain acyl-CoA dehydrogenase (LCAD), and acyl-CoA dehydrogenase (MCAD). The qRT-PCR assay was performed to evaluate the expression of *Pparpgc1α, Tfam, Lcad,* and *Mcad*. Data were expressed as mean ±SD (n=6); **p<0.01, ***p<0.001, ****p<0.001.

one-way analysis of variance with the Tukey's multiple comparisons test. All data were presented as means ± SD; *p*-values of <0.05, <0.01, and <0.001 were considered statistically significant.

Results

Emodin improved UUO-induced renal injury and fibrosis

To explore the effect of emodin on renal fibrosis, a UUO rat model was established. Fenofibrate has great inhibitory effects against tubulointerstitial fibrosis and inflammation.[26] Hence, it can be a positive control in this study. Histopathological abnormalities in the kidney tissues were investigated *via* H&E staining and Masson's trichrome staining. Results showed that emodin and fenofibrate treatment significantly relieved renal histopathological lesions caused by UUO and improved pathological scores. The vehicle treatment group presented with severe tissue degeneration and vacuole (Figure 1A). Masson's trichrome staining showed that both fenofibrate and emodin improved UUO-induced renal fibrosis in the tubules (Figure 1B). Furthermore, the levels of fibronectin, α-SMA, and COL1A1 were measured to evaluate renal fibrosis. As shown in Figure 1 C-E, the UUO-induced vehicle rats had high-

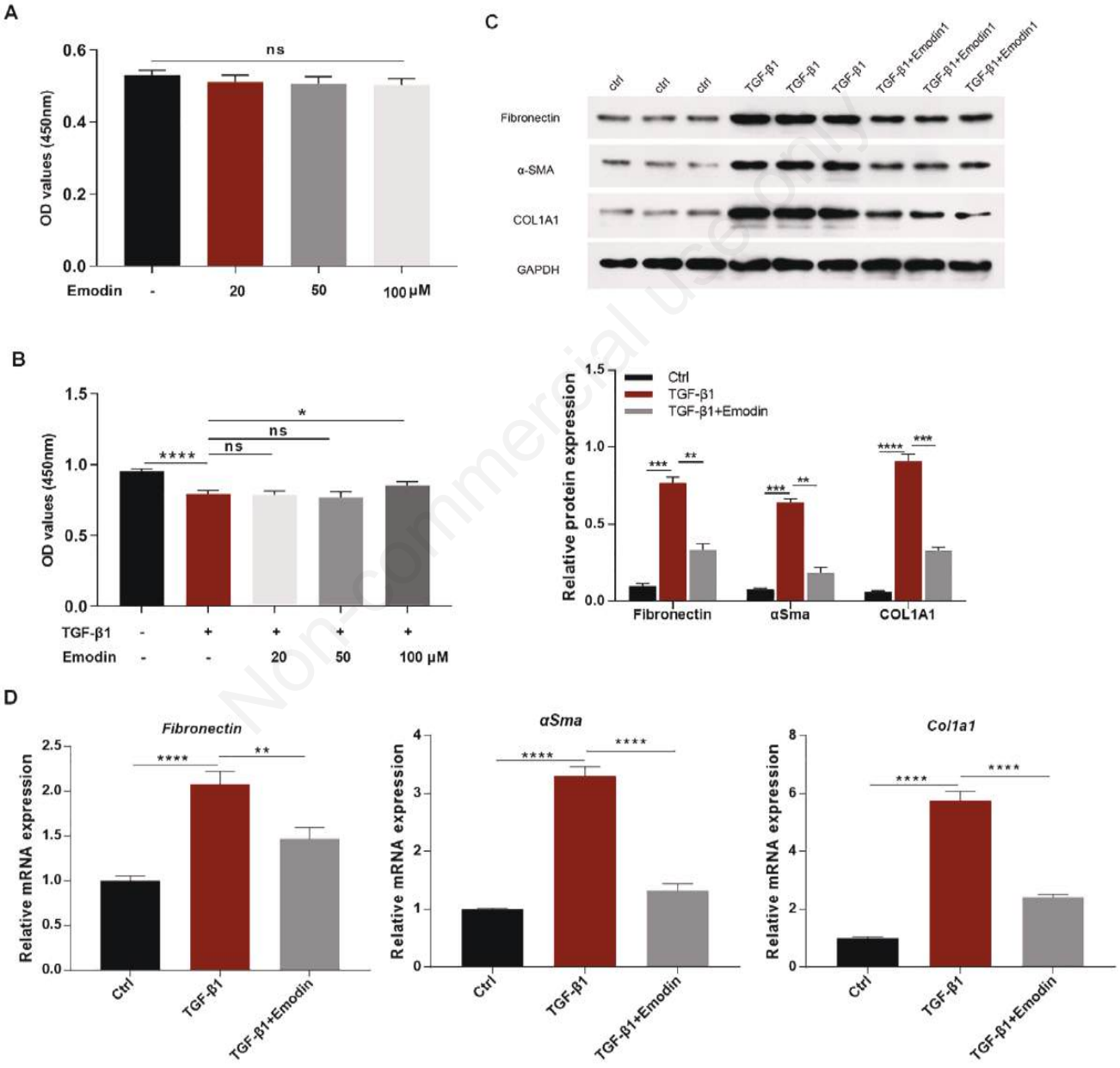

Figure 3. Emodin suppressed TGF-β1-induced cell fibrosis. Cell viability in emodin-treated NRK-52E cells without (**A**) or with (**B**) TGF-β1 stimulation was determined using the CCK-8 assay. **C**) Expression of fibronectin, α-SMA, and COL1A1 in NRK-52E cells was detected *via* Western blot analysis. **D**) The mRNA expression of *fibronectin, α-SMA, and Col1a1* was determined. Data were expressed as mean ±SD (n=3); ***p*<0.01, ****p*<0.001, *****p*<0.001.

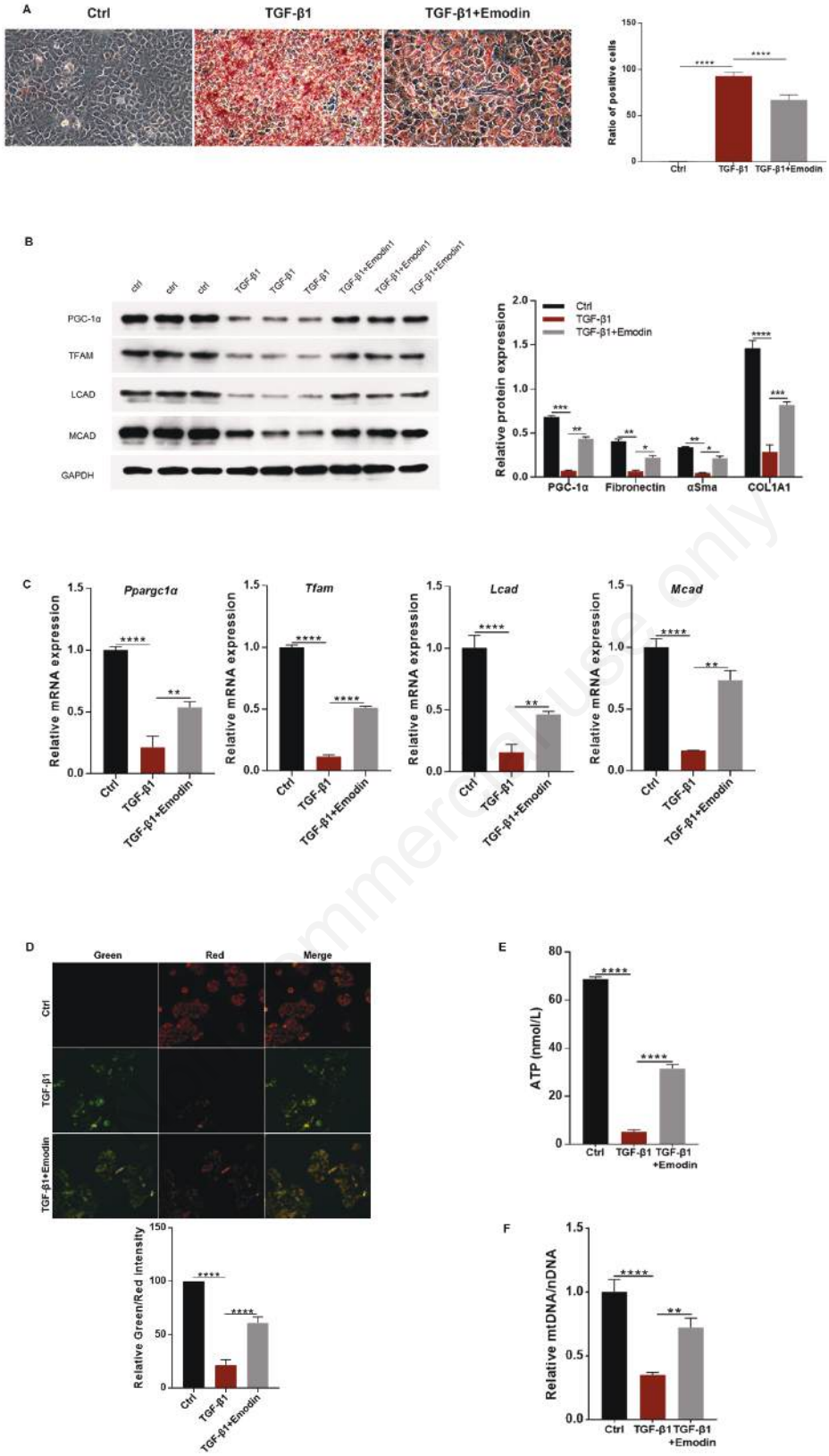

Figure 4. Emodin improved mitochondrial homeostasis in TGF-β1-induced cells. **A**) Oil Red O staining was performed to evaluate lipid accumulation in NRK-52E cells. **B**) Western blot analysis examined the expression of PGC-1α, Tfam, LCAD, and MCAD in NRK-52E cells, and the quantification of gray values. **C**) The mRNA expression of *Pparpgc1α, Tfam, Lcad*, and *Mcad* was assessed. **D**) Representative images and the quantification of mitochondrial membrane potential tested using the JC-1 probe. **E**) The ATP levels in NRK-52E cells after TGF-β1 induction and emodin treatment. **F**) The qRT-PCR assay was performed to quantify mitochondrial DNA levels using 16s rRNA and 18s rRNA primers. Data were expressed as mean ±SD (n=3); *p<0.05, **p<0.01, ***p<0.001, ****p<0.001.

er protein levels of fibronectin, α-SMA, and COL1A1 than sham controls. Meanwhile, the expression of these biomarkers was attenuated in emodin- and fenofibrate-treated rats. The mRNA expression of fibronectin, α–Sma, and Col1a1 decreased in UUO-induced rats after emodin or fenofibrate treatment.

Emodin facilitated mitochondrial homeostasis in UUO-induced rats

To investigate the effect of emodin on mitochondrial homeostasis, the expression of PGC-1 α and Tfam was evaluated. Results showed that the positive signals in emodin- and fenofibrate-treated rats were remarkably enhanced compared with those in vehicle-treated rats (Figure 2 A,B). LCAD and MCAD are two important fatty acid β-oxidation (FAO) enzymes involved in fatty acid metabolism in the mitochondria, which have been recently reported to be associated with renal function protection.[27,28] Results showed that emodin or fenofibrate treatment significantly increased the LCAD and MCAD expression in UUO-induced rats, thereby indicating that emodin had promising effects on fatty acid metabolism in the kidney (Figure 2 C,D). Furthermore, the mRNA level of *Pparpgc1α, Tfam, Lcad, and Mcad* in emodin- or fenofibrate-treated rats was upregulated compared with that in vehicle-treated rats, which is consistent with the immunohistochemistry results (Figure 2E).

Emodin suppressed TGF-β1-induced cell fibrosis

To evaluate the antifibrotic effects of emodin *in vitro*, we first explored the effects of emodin on NRK-52E cell viability using the CCK-8 assay. As shown in Figure 3A, emodin at different concentrations (25, 50, and 100 μM) had no significant effect. TGF-β1 significantly damaged the viability of NRK-52E cells , while emodin inhibited this detrimental effect (Figure 3B). The fibronectin, α-SMA, and COL1A1 expression of the TGF-β1 group significantly increased. Meanwhile, this effect was regulated by emodin treatment (Figure 3C). The mRNA level of *fibronectin, α- SMA, and Col1a1* was similar to the protein level (Figure 3D).

Emodin improved mitochondrial homeostasis in TGF-β1-induced NRK-52E cells

We further investigated the regulatory effect of emodin on mitochondrion homeostasis in NRK-52E cells. Lipid accumulation enhances the progression of renal fibrosis.[29] In the current study, Oil Red O staining was performed, and results showed that lipid droplets primarily accumulated in TGF-β1-induced cells. However, emodin-treated cells had a lower number of cells stained with Oil Red O (Figure 4A). The protein and mRNA levels of PGC-1 α, Tfam, LCAD, and MCAD in emodin-treated cells were higher than those in TGF-β1-treated cells (Figure 4 B,C). The mitochondrial membrane plays an important role in maintaining the respiratory chain to produce ATP. Hence, it was tested using a specific type of fluorescent probe, JC-1. As expected, the mitochondrial membrane potential was remarkably reduced by TGF-β1. Meanwhile, emodin treatment increased the membrane potential (Figure 4D). Thereafter, the ATP levels in the cytoplasm were measured. Results showed that TGF-β1-induced cells had a lower ATP level than control cells. However, the cells recovered their ability to generate ATP after emodin treatment (Figure 4E). Furthermore, emodin significantly increased the mtDNA-to-nDNA ratio, which was downregulated due to TGF-β1 induction (Figure 4F). In terms of ultrastructural morphology, the renal cells

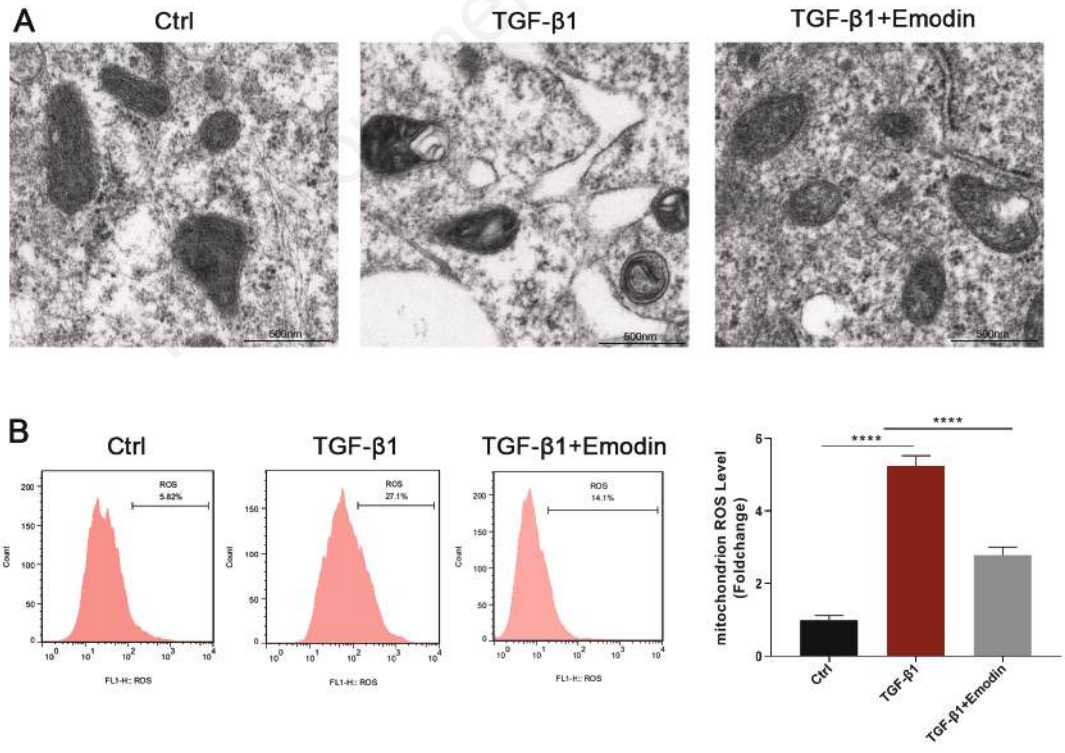

Figure 5. Emodin improved mitochondrial homeostasis in TGF-β1-induced cells. **A**) The ultrastructural morphology of NRK-52E cells was examined via transmission electron microscopy. **B**) ROS levels were detected by flow cytometry. Data were expressed as mean ±SD (n=3); ***p*<0.01, ****p*<0.001, *****p*<0.001.

of the control group had a normal rounded or rod-shaped mitochondria and regular arrangement of mitochondrial cristae. The TGF-β1 group had a swollen mitochondria with disorganized and fragmented cristae. However, this effect was reversed by emodin treatment (Figure 5A). In addition, the TGF-β1 group exhibited high intra-mitochondrial ROS levels, and this effect was decreased with emodin treatment (Figure 5B).

Emodin improved TGF-β1-induced fibrosis by upregulating the expression of PGC-1 α

A previous study has revealed that TGF-β1 reduced PGC-1α expression *via* Smad3, thereby lowering FAO and lipid accumulation.[30] To understand whether PGC-1α can be a target of emodin in regulating mitochondrial homeostasis and renal fibrosis, we knocked down PGC-1α with a specific siRNA. As shown in Figure 6, the expression of fibrosis-related proteins, such as fibronectin, α-SMA, and COL1A1, decreased in emodin-treated cells. Meanwhile, the expression significantly increased after PGC-1α knockdown. Consistently, the downregulation of fibrosis-associated genes in the emodin group was significantly reversed by silencing PGC-1α. Taken together, these results confirmed that the inhibitory effect of emodin against renal fibrosis was achieved by regulating PGC-1α.

Discussion

In the current study, emodin treatment not only improved mitochondrial function but also hampered aberrant histopathological alternation observed in UUO-induced rats. *In vitro*, it inhibited mitochondrial impairment, lipid accumulation, and renal fibrosis in TGF-β1-induced NRK-52E cells. Mechanistically, emodin improved mitochondrial function by upregulating PGC-1α expression, which protects cells against fibrosis. Collectively, our data showed that emodin is a promising antifibrotic candidate in the development of CKD.

Increasing evidence revealed that mitochondria dysfunction was commonly observed in CKD progression characterized by aberrant mitochondrial morphology, enhanced mitochondrial oxidative stress, and reduced mitochondrial biogenesis and ATP production.[31] PGC-1α is a nuclear coactivator of the peroxisome proliferator-activated receptor-γ, a member of PGC-1 family that

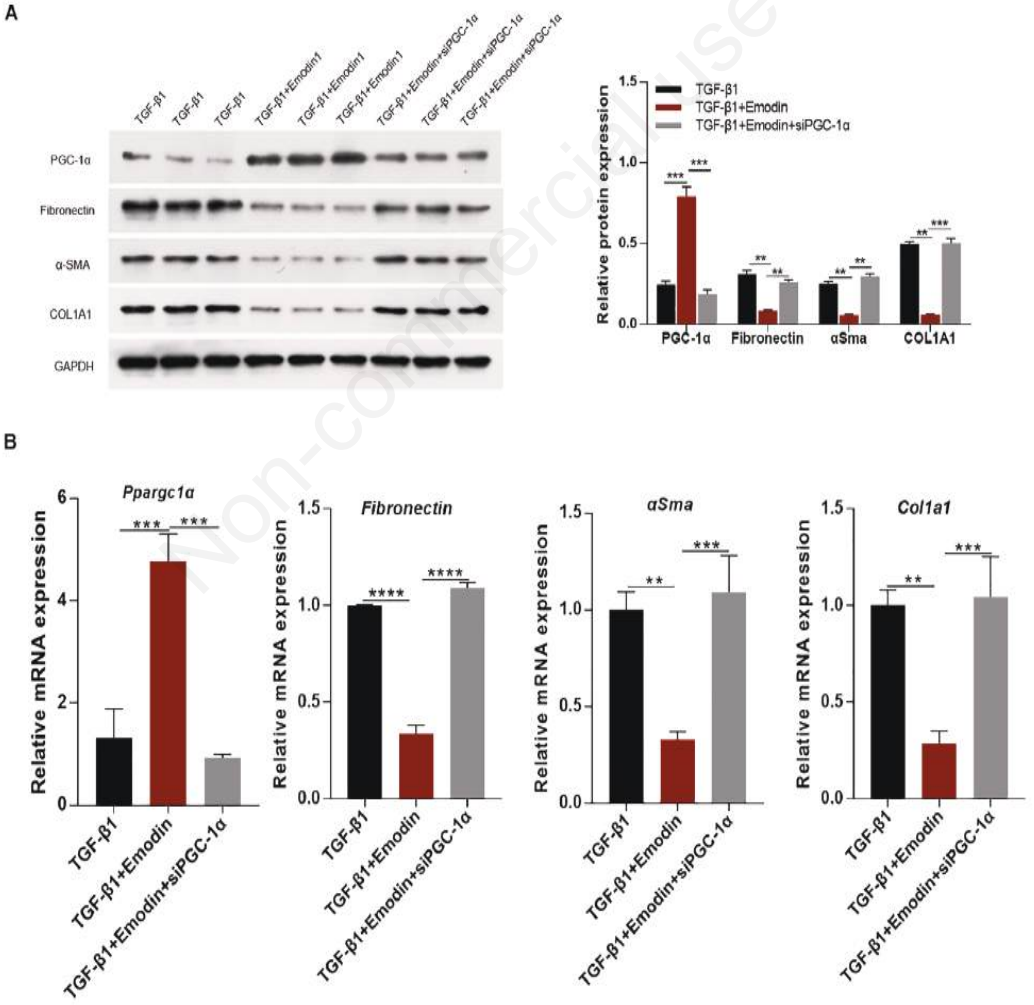

Figure 6. Emodin improved TGF-β1-induced fibrosis by upregulating PGC-1 α. **A**) Protein levels of PGC-1 α, fibronectin, α-SMA, and COL1A1 in TGF-β1-induced NRK-52E cells after emodin and PGC-1α knockdown treatment were determined. **B**) mRNA levels of *Pparpgc1α, Fibronectin, α-Sma,* and *Col1a1* were detected. Data were expressed as mean ±SD (n 3); ***p*<0.01, ****p*<0.001, *****p*<0.001.

can regulate mitochondrial biogenesis during cell proliferation.[32,33] PGC-1α can activate transcription and regulate downstream pathway by binding to response elements of other receptors.[34,35] When cells response to stimulus, such as glucose deprivation, starvation, and exercise, cytoplasm PGC-1α is translocated into nucleus. This activates nuclear respiratory chain factors 1 and 2, the transcription of the nuclear-coded respiratory chain, and Tfam, driving mitochondrial DNA transcription.[36] In addition, PGC-1α affected both fatty acid uptake and FAO in cells.[37] Maintaining the metabolic balance of fatty acids is one of important mitochondria's functions, which prevent intracellular deposition and protect cells from fibrotic progression.[38] In the current study, emodin-treated rats had a higher mRNA and protein level of Tfam and PGC-1α than UUO-induced model group. Meanwhile, the expression of FAO-associated proteins, including LCAD and MCAD, was decreased in both UUO-induced rats and TGF-β1-induced cells. Furthermore, emodin improved the mitochondrial homeostasis in TGF-β1-induced NRK-52 cells. This cascade demonstrates that the great effect of emodin in inhibition of lipid accumulation and mitochondrial dysfunction.

In a clinical study of CKD, the downregulation of PGC-1α and PGC-1α-associated mitochondrial gene expression was observed in the kidneys of patients with renal fibrosis.[19] Fibrosis is a key pathological process in CKD and a specific feature for evaluating renal disorders. PGC-1α was significantly decreased in renal fibrosis, exhibiting lipid accumulation and impaired FAO.[30] In this study, emodin improved UUO-induced fibrosis in rats and significantly downregulated the expression of fibrosis biomarkers. After silencing PGC-1α, the effects of emodin on these fibrosis-related proteins were reversed. This suggests that PGC-1α is required to improve mitochondrion function and fibrosis in emodin-treated cells.

In conclusion, emodin has a potent antifibrotic effect against UUO- and TGF-β1-induced renal fibrosis by maintaining mitochondrial homeostasis. Our findings indicate that emodin may act as a potential antifibrotic target against CKD development.

Acknowledgments

The authors would thank Jingwei Zhou for his critical contribution to the revision of the manuscript. The authors would also thank the Shenzhen Hospital of Beijing University of Traditional Chinese Medicine for providing support for this study.

References

1. Lv JC, Zhang LX. Prevalence and disease burden of chronic kidney disease. Adv Exp Med Biol 2019;1165:3-15.
2. Kovesdy CP. Epidemiology of chronic kidney disease: an update 2022. Kidney Int Suppl (2011) 2022;12:7-11.
3. Matsushita K, van der Velde M, Astor BC, Woodward M, Levey AS, de Jong PE, et al. Association of estimated glomerular filtration rate and albuminuria with all-cause and cardiovascular mortality in general population cohorts: a collaborative meta-analysis. Lancet 2010;375:2073-81.
4. Mazzuchi N, Schwedt E, Sola L, Gonzalez C, Ferreiro A. Risk factors and prevention of end stage renal disease in Uruguay. Ren Fail 2006;28:617-25.
5. Liu Y. Cellular and molecular mechanisms of renal fibrosis. Nat Rev Nephrol 2011;7:684-96.
6. Wei L-B, Ma Z-G, Ye R-G, Chen B-T, Zhan S-C, Huang H. Progress of intervention of renal interstitial fibrosis with Chinese traditional herbal medicine. Di Yi Jun Yi Da Xue Xue Bao 2002;22:946-8.
7. Muñoz-Félix JM, Martínez-Salgado C. Dissecting the involvement of Ras GTPases in kidney fibrosis. Genes (Basel) 2021;12:800.
8. Nogueira A, Pires MJ, Oliveira PA. Pathophysiological mechanisms of renal fibrosis: a review of animal models and therapeutic strategies. In Vivo 2017;31:1-22.
9. Chevalier RL, Forbes MS, Thornhill BA. Ureteral obstruction as a model of renal interstitial fibrosis and obstructive nephropathy. 2009;75:1145-52.
10. Martínez-Klimova E, Aparicio-Trejo OE, Tapia E, Pedraza-Chaverri J. Unilateral ureteral obstruction as a model to investigate fibrosis-attenuating treatments. Biomoleculs 2019;9:141.
11. Boor P, Ostendorf T, Floege J. Renal fibrosis: novel insights into mechanisms and therapeutic targets. Nat Rev Nephrol 2010;6:643-56.
12. Liu Y. Renal fibrosis: new insights into the pathogenesis and therapeutics. Kidney Int 2006;69:213-7.
13. Eddy AA. Molecular basis of renal fibrosis. Pediatr Nephrol 2000;15:290-301.
14. Ma TT, Meng XM. TGF-beta/Smad and renal fibrosis. Adv Exp Med Biol 2019;1165:347-64.
15. Martinez-Klimova E, Aparicio-Trejo OE, Gomez-Sierra T, Jimenez-Uribe AP, Bellido B, Pedraza-Chaverri J. Mitochondrial dysfunction and endoplasmic reticulum stress in the promotion of fibrosis in obstructive nephropathy induced by unilateral ureteral obstruction. Biofactors 2020;46:716-33.
16. Scarpulla RC. Metabolic control of mitochondrial biogenesis through the PGC-1 family regulatory network. Biochim Biophys Acta 2011;1813:1269-78.
17. Nam BY, Jhee JH, Park J, Kim S, Kim G, Park JT, et al. PGC-1alpha inhibits the NLRP3 inflammasome via preserving mitochondrial viability to protect kidney fibrosis. Cell Death Dis 2022;13:31.
18. Chambers JM, Wingert RA. PGC-1alpha in disease: recent renal insights into a versatile metabolic regulator. Cells 2020;9:2234.
19. Han SH, Wu MY, Nam BY, Park JT, Yoo TH, Kang SW, et al. PGC-1alpha protects from notch-induced kidney fibrosis development. J Am Soc Nephrol 2017;28:3312-22.
20. HaoShang, Jia X, Liu H, Zhang X, Shao Y. A comprehensive review of emodin in fibrosis treatment. Fitoterapia 2023;165:105358.
21. Ma L, Li H, Zhang S, Xiong X, Chen K, Jiang P, et al. Emodin ameliorates renal fibrosis in rats via TGF-beta1/Smad signaling pathway and function study of Smurf 2. Int Urol Nephrol 2018;50:373-82.
22. Yang F, Deng L, Li J, Chen M, Liu Y, Hu Y, Zhong W. Emodin retarded renal fibrosis through regulating HGF and TGFbeta-Smad signaling pathway. Drug Des Devel Ther 2020;14:3567-75.
23. Xu L, Gao J, Huang D, Lin P, Yao D, Yang F, et al. Emodin ameliorates tubulointerstitial fibrosis in obstructed kidneys by inhibiting EZH2. Biochem Biophys Res Commun 2021;534:279-85.
24. Meng X-M, Nikolic-Paterson DJ, Lan HY. TGF-β: the master regulator of fibrosis. Nat Rev Nephrol 2016;12:325-38.
25. Tanaka Y, Kume S, Araki S, Isshiki K, Chin-Kanasaki M, Sakaguchi M, et al. Fenofibrate, a PPARalpha agonist, has renoprotective effects in mice by enhancing renal lipolysis. Kidney Int 2011;79:871-82.
26. Li L, Emmett N, Mann D, Zhao X. Fenofibrate attenuates tubulointerstitial fibrosis and inflammation through suppres-

sion of nuclear factor-κ B and transforming growth factor-β 1/Smad3 in diabetic nephropathy. Exp Biol Med (Maywood) 2010;235:383-91.
27. Kurtz DM, Rinaldo P, Rhead WJ, Tian L, Millington DS, Vockley J, et al. Targeted disruption of mouse long-chain acyl-CoA dehydrogenase gene reveals crucial roles for fatty acid oxidation. Proc Natl Acad Sci USA 1998;95:15592-7.
28. Hu G, Xu L, Ma Y, Kohzuki M, Ito O. Chronic exercise provides renal-protective effects with upregulation of fatty acid oxidation in the kidney of high fructose-fed rats. Am J Physiol Renal Physiol 2020;318:F826-34.
29. Gai Z, Wang T, Visentin M, Kullak-Ublick GA, Fu X, Wang Z. Lipid accumulation and chronic kidney disease. Nutrients 2019;11:722.
30. Kang HM, Ahn SH, Choi P, Ko YA, Han SH, Chinga F, et al. Defective fatty acid oxidation in renal tubular epithelial cells has a key role in kidney fibrosis development. Nat Med 2015;21:37-46.
31. Zschiedrich S, Bork T, Liang W, Wanner N, Eulenbruch K, Munder S, et al. Targeting mTOR signaling can prevent the progression of FSGS. J Am Soc Nephrol 2017;28:2144-57.
32. Villena JA. New insights into PGC-1 coactivators: redefining their role in the regulation of mitochondrial function and beyond. FEBS J 2015;282:647-72.
33. Tontonoz P, Hu E, Spiegelman BM. Stimulation of adipogenesis in fibroblasts by PPAR gamma 2, a lipid-activated transcription factor. Cell 1994;79:1147-56.
34. Puigserver P, Wu Z, Park CW, Graves R, Wright M, Spiegelman BM. A cold-inducible coactivator of nuclear receptors linked to adaptive thermogenesis. Cell 1998;92:829-39.
35. Lin J, Handschin C, Spiegelman BM. Metabolic control through the PGC-1 family of transcription coactivators. Cell Metab 2005;1:361-70.
36. Fontecha-Barriuso M, Martin-Sanchez D, Martinez-Moreno JM, Monsalve M, Ramos AM, Sanchez-Nino MD, et al. The role of PGC-1alpha and mitochondrial biogenesis in kidney diseases. Biomolecules 2020;10:347.
37. Miguel V, Tituaña J, Herrero JI, Herrero L, Serra D, Cuevas P, et al. Renal tubule Cpt1a overexpression protects from kidney fibrosis by restoring mitochondrial homeostasis. J Clin Invest 2021;131:e140695.
38. Afshinnia F, Rajendiran TM, Soni T, Byun J, Wernisch S, Sas KM, et al. Impaired β-oxidation and altered complex lipid fatty acid partitioning with advancing CKD. J Am Soc Nephrol 2018;29:295.

Received: 20 November 2023. Accepted: 27 March 2024.

European Journal of Histochemistry 2024; 68:3917
doi:10.4081/ejh.2024.3917